Acta Cryst. (1970). A**26**, 613

Simple Estimates of the Thermal Diffuse Scattering Contribution to Bragg Peaks

BY L. D. JENNINGS

Army Materials and Mechanics Research Center, Watertown, Massachusetts,

(*Received* 20 *October* 1969)

The thermal diffuse scattering (TDS) contribution to X-ray Bragg peaks is discussed in terms of its two experimental components, the included and the background parts. The discussion is primarily directed toward situations where detailed elastic constant information and a large computer are not available. Graphs are displayed which, in the spherical average approximation, allow an accurate assessment of the influence of all the experimental variables on the TDS contribution. It is shown that, even in the general case where spherical averaging is a poor approximation, the included TDS varies linearly with length of scan for small scans. A technique for determining the constant of proportionality is suggested. Thus the included TDS may be evaluated even though the elastic constants are not known.

1. Introduction

The measurement of an integrated Bragg reflection will in general contain an unwanted component due to thermal diffuse scattering (TDS). A nearly exact expression for the TDS has been known for many years (*e.g.* James, 1948), but only recently have there been serious analytical and numerical approximations to the integrals required to apply this expression to an evaluation of the unwanted component (Walker & Chipman, 1970; Rouse & Cooper, 1969; and other references given by these authors). Although these authors have given methods for calculating the TDS contribution with great accuracy in specific cases, they have not presented their results in such a way as to make clear how these results depend on the various experimental parameters, except in a limited number of examples. Similarly, their results are not easily adaptable to making a rapid approximation to the correct value.

We will show that it is most convenient to consider the total TDS fraction in terms of its two experimental constituents, the included part and the background (or slit) part. We present graphs which allow an estimate of each of these parts and which show clearly the influence of the various experimental parameters. An understanding of the geometrical basis of these graphs permits their extension to many cases not explicitly covered and also suggests a technique for evaluating the included TDS in cases where information about the velocity of sound is not available.

2. Formulation

If an ideally mosaic single crystal is scanned through a Bragg reflection, the total TDS fraction, α_T (defined as the ratio of the total integrated thermal diffuse power to the integrated Bragg power), is approximately (Cochran, 1969; Walker & Chipman, 1970)

$$\alpha_T = \frac{L}{\pi}\int \frac{\lambda K_H(\chi)\mathrm{d}V}{K_{\mathrm{avg}}\, q^2} . \qquad (1)$$

The integral is over the active volume in reciprocal space as shown in Fig. 1. A position in reciprocal space is defined by its distance q and direction χ from the reciprocal lattice point (relp) H. Such a direction is called a rekha by Ramachandran & Wooster (1951) and the associated parameter $K_H(\chi)$ is called the rekha constant. It is defined in terms of the sound velocities associated with the rekha χ. In a typical experimental arrangement, the principle approximation in equation (1) is the neglect of the necessary convolution arising from geometry, wavelength spread and mosaicity; the other approximations, such as the restriction to first order TDS, become exact in the limit of small scans and involve corrections of a few per cent in typical cases. The parameter L is given by

$$L = 4\pi \sin^2\theta\, k_B T\, K_{\mathrm{avg}}/\lambda^3 . \qquad (2)$$

The approximation does not distinguish the scattering angle 2θ from the double Bragg angle. The average energy per vibrational mode is k_BT and K_{avg} is obtained by averaging $K_H(\chi)$ over all rekhas. This procedure requires a knowledge of the elastic constants, and is discussed in detail elsewhere (Rouse & Cooper, 1970; Walker & Chipman, 1969). If detailed elastic constant data are not available, K_{avg} may be expressed as $1/\varrho V_{\mathrm{avg}}^2$, with ϱ the density and V_{avg} an average sound velocity. (See §§ 4 to 6).

As first shown by Skelton & Katz (1969), a great simplification of equation (1) may be effected through application of the divergence theorem.

$$\alpha_T = \frac{L}{\pi}\int \lambda g \frac{K_H(\chi)}{K_{\mathrm{avg}}}\,\mathrm{d}\chi . \qquad (3)$$

Here g is the distance to the surface of the active volume along the rekha χ, and the integral is carried out over all elements of solid angle. In the case that the surface of the active volume is composed of a number of plane surfaces, it is convenient to re-express this:

$$\alpha_T = \frac{L}{\pi}\int_T \lambda n \frac{K_H(\chi)}{K_{\mathrm{avg}}}\,\frac{\mathrm{d}A}{g^2} \qquad (4)$$

where n is the normal distance from the relp to the element of surface area, and the integral is carried out over the total bounding surface shown in Fig. 1.

The values of α_T are not the most interesting quantities from a practical point of view. Almost always one wants the amount of TDS power included after making an integrated background subtraction; the most usual technique is to multiply the average power at the ends of the scan by the time required to carry out the scan. Although it is easy to generalize to asymmetric scans, the notation is simplified by restriction to scans symmetric about the relp. The integrated background, expressed as a fraction of the integrated Bragg reflection, is then found to be given by an expression identical with equation (4), except that the integral is carried out over only the slit surface depicted in Fig. 1. We therefore denote this quantity by α_S, which is also a convenient measure of the TDS power (for an example of such usage, see Jennings, 1969). Finally, the fraction of TDS included in a usual Bragg scan α_I is given again by the same integral, but over the included surface defined in Fig. 1. The geometric interpretation of the α's is given in Fig. 3(a); they are related by $\alpha_T=\alpha_I+\alpha_S$. The components are not only simpler but more important than the total: the included fraction is needed to correct observed Bragg intensities, and the slit fraction may be used to assess the accuracy of the model being used, or even to obtain elastic constants.

The values of the α's depend on the angular height and width of the receiving slit, h and w; the total angle of crystal rotation, Ω; the type of scan, defined by the angle ψ; the scattering angle, 2θ; and the angular dependence of the rekha constant, $K_H(\chi)$. In spite of this imposing array of variables, it is possible, with the aid of a geometric understanding of the situation and a few appropriate graphs, to make a rapid, meaningful estimate of the more important required values. To this end, we consider the situation in the spherical average approximation: we assume that $K_H(\chi)$ is given by K_{avg}, independent of χ. This situation is identical with that considered by Skelton & Katz (1969) and by Cooper & Rouse (1968) and all the results of these authors may be obtained from the graphs which we will present (except that Cooper & Rouse (1968) consider a less usual type of background correction).

In the case of symmetric scans, the required integrals may be reduced to a dimensionless form. It is usually most convenient to use the slit width as the most important parameter, in which case we may summarize the situation by stating our working formula

$$\frac{\alpha_i}{Lw}=\frac{1}{\pi}\int_i \frac{\lambda n}{w}\frac{\mathrm{d}A}{g^2}, \qquad (5)$$

where the i indicates either the slit surface or the included surface and the integral depends only on the shape parameters: h/w, $\Omega \sin 2\theta/w$, and ψ. In the Appendix, the integrals are detailed in a form suitable for numerical integration.

3. Calculation of TDS fraction

Consider first the case of a square receiving slit: $h/w=1$. From equation (5) we may then calculate α_S and α_I as a function of $\Omega \sin 2\theta/w$ for various values of ψ, as shown by the solid curves in Fig. 2. Within the stated approximations, these curves depict both the included and the slit TDS fractions for any combination of slit width, length of scan, type of scan, and scattering angle. Thus one may see, in greater generality than in previous treatments, the influence of the various experimental parameters.

The main features of the curves of Fig. 2 arise from the geometry of the active volume, particularly whether the included or slit surface is nearer the relp. Once these features are understood, it is possible to interpolate the curves of Fig. 2 to an accuracy compatible with the other approximations, *i.e.* about 10%. It is first important to distinguish between cases where the slit moves more nearly normal to the Ewald sphere during the scan and those where it moves more nearly tangentially, *i.e.* whether ψ is greater or less than 45°. The former case is completely contained in the small region between the curves A and B in the Figure. If one notes, in addition, the asymptotic behavior

$$\frac{\alpha_S}{Lw}=\frac{(4/\pi)\,(h/w)\sin^2\psi}{\Omega \sin 2\theta/w} \quad (\text{for large } \Omega), \qquad (6)$$

it is clear that the necessary interpolations may be made easily. Normal scans ($\psi=90°$) are of interest because

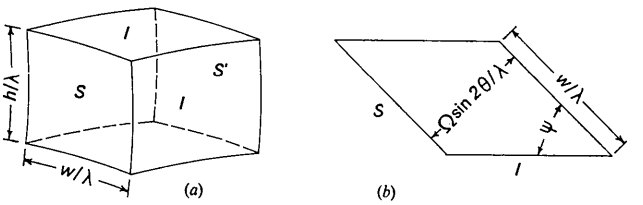

Fig. 1. Depiction of the active volume. The surface S is that portion of the Ewald sphere containing rays which are accepted by the slit, which is assumed rectangular with an angular height and width of h and w. During a scan the Ewald sphere moves so that S is at a new position S'. We refer to either or both of these surfaces as the slit surface, or even as the slit. The boundaries of the slit generate four faces, which together form the included surface I. The region between S and S' is the active volume V and its total surface is called T. In the case that the active volume is small, the bounding surfaces are approximately planar as shown in cross section in (b). During the scan the sample rotates an amount Ω with respect to the incident beam, and ψ defines how the slit moves with respect to the Ewald sphere during the scan. By viewing the origin of the reciprocal lattice as being either below or to the side of the Figure, ψ may be restricted to the range 0–90°. For an ω:2θ scan (radial in reciprocal space), $\psi=\theta$, the Bragg angle. For an ω scan (constant radius in reciprocal space), $\psi=90°-\theta$. For symmetrical scans the relp is centered on the Figure.

they give the most compact active volume; even if one has only a choise between ω and $\omega{:}2\theta$ scans, it is always possible to arrange a more nearly normal condition ($\psi > 45°$).

The nearly tangential case, $\psi < 45°$, is more complicated, and we discuss, for simplicity, the case $\sin 2\psi = \sin 2\theta$. This discussion applies to an $\omega{:}2\theta$ scan with $\psi = \theta$ or to an ω scan with $\psi = 90° - \theta$. (The active volumes in the two cases are identical; only the orientations with respect to the origin differ.) The prominent feature of the nearly tangential case is the break occurring near $\Omega/w = \frac{1}{2}$. If, therefore, each curve is translated by a factor of $\sin 2\theta$ along each coordinate axis, the breaks are nearly superposed, and interpolation becomes simple. This procedure is illustrated for the included fraction in the insert to Fig. 2(*b*).

From the curves, one may easily discern the dependence of the TDS fractions on the experimental conditions. For example, since $\omega{:}2\theta$ and ω scans are described by complementary values of ψ, one such

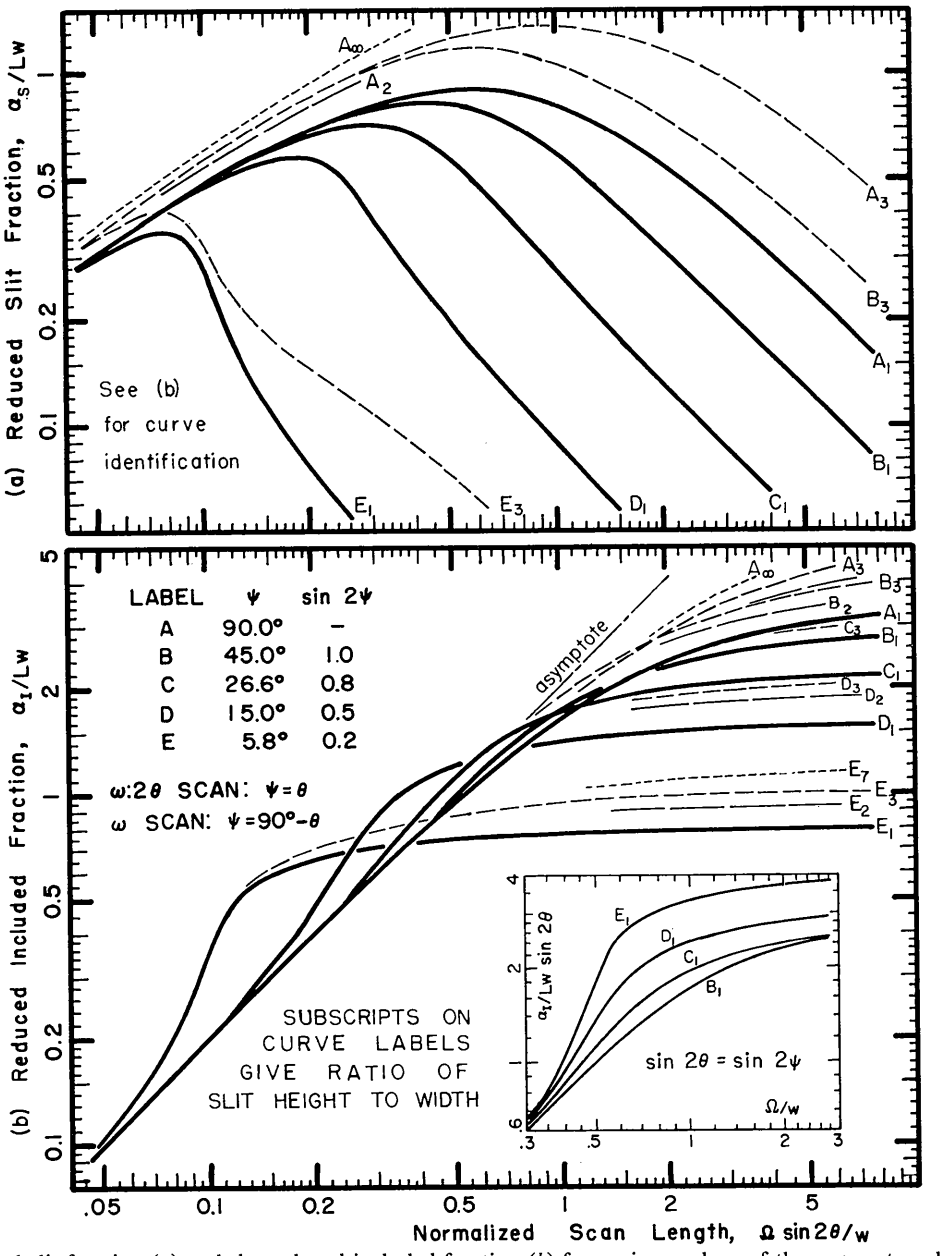

Fig. 2. The reduced slit fraction (*a*) and the reduced included fraction (*b*) for various values of the parameters defined in Fig. 1. The insert in (*b*) applies to ω or $\omega{:}2\theta$ scans only, but is useful in nearly tangential cases. The curves are labeled by letters indicating the ψ value and by subscripts indicating the ratio of slit height to width. For example, the short curve in the upper right of (*b*), whose label is omitted because of space limitations, would be referred to as A_2: $\psi = 90°$, $h/w = 2$. The curve C_2 is obscured by B_1. Note the wide range of ψ values contained between the neighboring curves *A* and *B*.

scan is always described by a curve between A and B. The other scan is described by curves such as C, D, or E, and one may see that the included fraction is quite a different function of the parameters for the two types of scan.

The dependences on the length of scan Ω and on slit width w are intimately related. The Ω dependence can be determined directly from the curves. The w dependence may be visualized by shearing the curves 45° and reading from right to left; *i.e.* where α varies as Ω^m, it also varies as w^{1-m}. We may, for example, distinguish different regions for the included fraction. At small Ω, α_I varies linearly with Ω and is independent of w. In the nearly tangential case only, there is a region of very strong dependence on Ω and inverse dependence on w. Finally, for large scans, α_I varies linearly with w and is independent of Ω.

In contrast to the slit width, which is important because of its influence on the tangential case, the slit height is important only for large scans, where the slit area comes into play. [See equation (6).] Although such large scans might not be important in practice, we have shown enough cases in Fig. 2 that interpolation to almost any slit size is possible.

The dependence on θ is contained in the explicit factor $\sin 2\theta$, in the fact that ψ depends on θ for the usual scan arrangements, and in the normalizing factor L. Equation (2) shows that L varies as $\sin^2\theta$, which is the same angular dependence as the exponent in the Debye–Waller factor. Thus one may simply determine the conditions under which the TDS correction may be incorporated with the temperature factor.

All the quantitative discussion has been within the spherical averaged approximation. Because of the distinction between longitudinal and transverse sound velocities, this approximation is not valid even for an isotropic material. However, the gross features of our results, which depend on geometrical considerations alone, will obtain even in the general case. The details will be changed, though. For example, the exact correspondence of ω and ω:2θ scans at complementary angles will be spoiled: in the approximately isotropic case, high angle scans are enhanced and low angle scans diminished for moderate scan lengths. Similarly, an ω:2θ scan is enhanced *vis-à-vis* an ω scan at the same angle.

Because of their simple form, the results given here may easily be convoluted with the various instrumental broadenings, either analytically or by visualization of the smearing of the active volume. The magnitude of these effects has been estimated by Cochran (1969) and by Walker & Chipman (1970). We confine our discussion to the example of § 5.

4. Small scans, anisotropic sample

It is seen, in Fig. 2(*b*), that the included fraction varies linearly with scan length for small scans. We now show that this simple result obtains in the most general case, not merely in the spherical approximation. For a small scan, the included surface forms a narrow band. The width of this band, projected on the normal to the Ewald sphere, is just $\Omega \sin 2\theta$. Assume that the band is so narrow that neither the rekha constant nor the distance from the relp changes appreciably across the band, *i.e.* $\Omega \sin 2\theta \ll w, \Omega \sin 2\theta/\tan\psi \ll w, \Omega \sin 2\theta \ll h$. (We do not preclude the case of an anisotropic sample or an irregular slit so that these quantities change *along* the band.) Then, if φ is the angular coordinate in the plane tangent to the Ewald sphere near the relp, we have from equation (3)

$$\alpha_I = \frac{L\Omega \sin 2\theta}{\pi} \int_0^{2\pi} \frac{K_H(\varphi)\mathrm{d}\varphi}{K_{\mathrm{avg}}} = 2L'\Omega \sin 2\theta \quad (\text{for small } \Omega), \tag{7}$$

where L' is identical to L, except that K_{avg} is replaced by the value K'_{avg}, which is K_H averaged over the plane tangent to the Ewald sphere. To give a feeling for the distinction, we note that for an isotropic material

$$K'_{\mathrm{avg}} = \frac{1}{\varrho}\left[\frac{1}{V_t^2} - \frac{\cos^2\theta}{2}\left(\frac{1}{V_t^2} - \frac{1}{V_l^2}\right)\right], \tag{8}$$

whereas

$$K_{\mathrm{avg}} = \frac{1}{3\varrho}\left[\frac{2}{V_t^2} + \frac{1}{V_l^2}\right]. \tag{9}$$

V_l and V_t are the longitudinal and transverse sound velocities. Note that, even for this simple model, K'_{avg} displays an angular dependence while K_{avg} cannot.

It should be noted that the restriction to small scans is not so limiting as might appear; any scan can be made 'small' through the use of a sufficiently large slit. So long as the scan is small, equation (7) applies independent of slit dimensions, of scan type parameter ψ, and of instrumental broadening as will be discussed later. In those cases for which it is applicable, equation (7) represents an enormous simplification over the more general (3) or (4) since, in the general case, the evaluation of each $K_H(\chi)$ requires the inversion of a 6×6 matrix. [See Rouse & Cooper (1969), equation (36) for the formula determining K_H.]

5. Experimental estimate of the TDS contribution

The foregoing discussion presumes at least some knowledge of the elastic constants or the velocity of sound. Depending on the availability of such information and on the accuracy required, it may not be feasible to use the simple methods discussed previously or even the most sophisticated computer calculation. For such cases, we suggest an experimental technique for estimating the TDS fraction, making use only of the same instrumentation required for the integrated reflection measurements.

No broadening

We make use of equation (7) as illustrated in Fig. 3(*a*), which is a graph of the TDS power for a monochromated collimated ray impinging on a small sample with negligible mosaic spread. The abscissa is the amount of sample rotation and the units of power and/or of angle are adjusted so that areas are expressed as fractions of the integrated Bragg reflection. In this case (no aberrations), the Bragg reflection would be very sharp, and the TDS fraction could be made negligible by use of a small scan. Nevertheless, suppose that we are restricted to scans larger than some minimum value, Ω_0. There would then be a minimum TDS contribution to the measured Bragg peak equal to the area A_0. If the usual background subtraction were made, the desired quantity would be $A_1 = A_0 - \Omega_0 P_0$. Since A_1 is related to A_0 by known quantities finding A_0 is tantamount to obtaining A_1. To find A_0, we make use of the relations displayed in Fig. 3(*a*) together with equation (7) to show that

$$E = A' - \Omega P = -A_0 + 2L'\Omega \sin 2\theta \text{ (for small } \Omega). \quad (10)$$

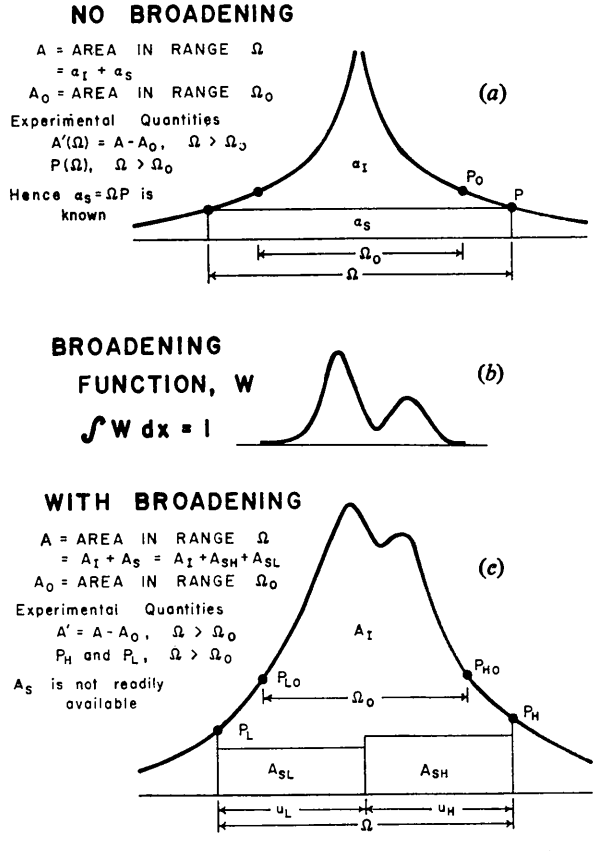

Fig. 3. Representations of the received power *vs.* crystal scan angle. (*a*) TDS power in the case of no experimental broadening. (*b*) Bragg diffracted power. The curve also represents the resolution function W. (*c*) The convolution of (*a*) and (*b*), representing the experimental TDS power. The region Ω_0 is unobservable because of interference from the much stronger Bragg reflection (*b*).

For $\Omega > \Omega_0$ the quantity E may be measured. Thus if E is plotted against Ω a straight line should result; the intercept is the desired unknown area, A_0, and the slope is related to the velocity of sound in the sample.

With broadening

In an actual experiment it is seldom possible to achieve negligible broadening from wavelength, mosaicity, beam divergence, *etc.* The effect of all these broadenings may be represented either by smearing the active volume around a fixed relp or by a fixed active volume around a smeared relp. We take the latter point of view. Thus to each point in a region around the nominal relp we attach a weight. We alternatively refer to this weighting function as the broadening or resolution function. A little reflection shows that so long as the slit is large compared to the divergences (the usual case), it is only the projection of the weighting function on the line traced by the center of the slit which is important. This projection W is thus easily measured as the normalized profile of the Bragg peak; an example is shown in Fig. 3(*b*). The actual received TDS power is then the convolution of Fig. 3(*a*) with Fig. 3(*b*), resulting in the curve of Fig. 3(*c*). The region Ω_0 would be obscured by the Bragg peak and the desired unknown area is again denoted by A_0. Because W may, in general, be asymmetric, it is necessary to distinguish the high and low angle sides of the curve by the subscripts H and L as indicated in the Figure. Expressing the situation analytically, we have

$$P_H = \int \frac{W(x)\alpha_S(2u_H - 2x)}{2u_H - 2x}\,dx \quad (11)$$

$$P_L = \int \frac{W(x)\,\alpha_S(2u_L + 2x)}{2u_L + 2x}\,dx \quad (12)$$

$$\begin{aligned} A &= A_I + A_{SH} + A_{SL} \\ &= \tfrac{1}{2}\{\textstyle\int W(x)[\alpha_I(2u_H - 2x) + \alpha_I(2u_L + 2x)]dx \\ &\quad + \textstyle\int W(x)\alpha_S(2u_H - 2x)dx + \int W(x)\alpha_S(2u_L + 2x)dx\} \end{aligned} \quad (13)$$

where α_I and α_S are given by equations (1), (3), or (4) but with the integration understood to be over the appropriate surface of the active volume. The explicit argument of the α's is the value of Ω in Fig. 1; the other parameters are understood.

The experimental determination of the unknown area A_0 is not nearly so simple in Fig. 3(*c*) as in Fig. 3(*a*) because the convolutions spoil the simple relationship between A_S and P. We wish first to suggest an approximate technique for this determination and then to give a few illustrations which will clarify the entire discussion.

Motivated by the simplicity of the analysis of Fig. 3(*a*), we rewrite equation (13),

$$A = 2(1-\varepsilon)L'\Omega \sin 2\theta + u_{CH}P_H + u_{CL}P_L \quad (14)$$

where each term is, by definition, taken equal to the corresponding term in equation (13). The lack of

information is thus thrown into the correction parameters ε, u_{CH}, and u_{CL}. These parameters could be evaluated as a function of the u_i ($i=L$ or H) if the α_i ($i=I$ or S) were known. Of course, this is not the case, but some information is known. For small Ω, ε approaches zero with zero slope. For a narrow weighting function, W, or a large scan, the u_{Ci} approach the corresponding u_i. Thus, assuming for the moment that ε, u_{CH}, and u_{CL} are known, we may write

$$A'+2\varepsilon L'\Omega \sin 2\theta - u_{CH}\, P_H - u_{CL} P_L = -A_0 + 2L'\Omega \sin 2\theta\,, \qquad (15)$$

evaluate the left hand side from the experimental data, and plot the result *versus* Ω as before. An iteration may be necessary because of the presence of L' on both sides of the equation, but this is not really the troublesome term.

Suggested approximation

The greatest difficulty in making use of equation (15) is the estimation of the u_{Ci}. Our proposal is that they be evaluated by replacing the unknown α_i in equations (11) to (13) by the corresponding quantities obtained using the spherical approximation. The necessary formulae are detailed in the Appendix.

Illustration

To assess the accuracy of this suggested approximation, one might compare its results with those obtained experimentally. It is at present, however, extremely difficult to obtain accurate experimental values for the TDS contained under a Bragg peak. Instead we have considered two samples which are taken to obey equation (1) exactly, one nearly isotropic and the other highly anisotropic.

We have examined three different weighting functions:

$W_1(x)=1-4|x|$, with x measured in degrees. This triangular function simulates the use of slits producing horizontal divergence of 0·5°, which would thus be the minimum scan length for W_1. ($W_1=0$ for $|x|>\frac{1}{4}$.)

$W^2(x)=\delta(x+0{\cdot}17°)+\delta(x-0{\cdot}17°)$. This function approximates the effect of a Mo $K\alpha$ doublet near $\theta=45°$. The minimum scan is 0·34°, but the bulk of the weight is nearer the surface of the active volume than for W_1.

W_3 is W_1 folded with 1° of vertical divergence. This folding has no influence on $W(x)$, but the simulated experimental data were calculated with the more general W_3.

Since each of these weighting functions is symmetric, we may drop the distinction between the two ends of the scan; thus we drop the subscripts H and L. It is of interest to consider three approximations to the unknown parameter in equation (15):

Approximation 0: $\varepsilon=0$; $u_C=u$.

Approximation 1: $\varepsilon=0$; $u_C=u_S$, the value obtained using the spherical approximation.

Approximation 2: Both ε and u_C obtained using the spherical approximation.

For each case, we could evaluate the simulated experimental data and also exact values for all parameters. Using the simulated data, we may evaluate the left hand side of equation (15) using any of the three approximations. Denote these values by E_0, E_1 and E_2. The effectiveness of the approximation could be displayed by plotting the E's *versus* Ω and seeing how well such plots yield the desired quantities A_0 and L'. The same information can be displayed in a more compact form, without any fundamental change, by adding the linear function $A_0-2L\Omega \sin 2\theta$ to each E. In this case the intercept should be zero and the slope $2(L'-L)\sin 2\theta$. Thus any deviation from a horizontal line displays the inadequacy of the spherical approximation ($L'=L$).

In Fig. 4 we have plotted illustrative cases of the technique described above. The ordinates are reduced by the factor Lw_0 so that they are directly comparable with those in Fig. 2; w_0 is the width of a standard slit, chosen as 3° for the example. Since, in these units, the included TDS is about unity for a typical length of scan, we note that an error of 0·1 in Fig. 4 represents about 10%. For each case, we show values obtained in each of the approximations (E_3 will be discussed later). The solid curve shows the behavior of E_0 or E_1 if u_C/u were chosen correctly. The dashed line shows the behavior of E_2 if u_C/u and ε were chosen correctly. In an actual experiment the information required to plot the curves would not be available, but that required to plot the points would be. The effectiveness of the proposed approximation is determined by the degree to which the sets of points may be extrapolated to a zero intercept.

A nearly isotropic case is represented in Fig. 4(*a*). Although an error of 10 – 20% might be anticipated with E_0, the error using E_1 or E_2 would surely be smaller than other experimental errors. Note that the distinction between longitudinal and transverse velocities gives rise to a nonzero initial slope and to the failure of E_2 to be exact at moderate scan lengths.

Fig. 4(*b*) and (*c*) represent two different sample orientations for a reflection chosen to show the largest deviations from the spherical approximation. The apparent linearity [in Fig. 4(*b*)] of E_1 out to large scans is a cancellation of the curvature toward the axis to be expected on account of anisotropy and the curvature downward to be expected on account of geometrical effects. This effect is shown again in Fig. 4(*c*) where the curvatures have the same sign. The error in intercept in either case would be less than 0·1, but one might have less confidence in case 4(*c*) because of the appreciable curvature at the smallest feasible scans. One would therefore make use of a larger slit as shown in Fig. 4(*d*). The initial slope can be determined with

far greater accuracy in this case. Then, since the initial slope must be the same for any slit size, the intercept for the standard slit [Fig. 4(*c*)] could be estimated more precisely than otherwise.

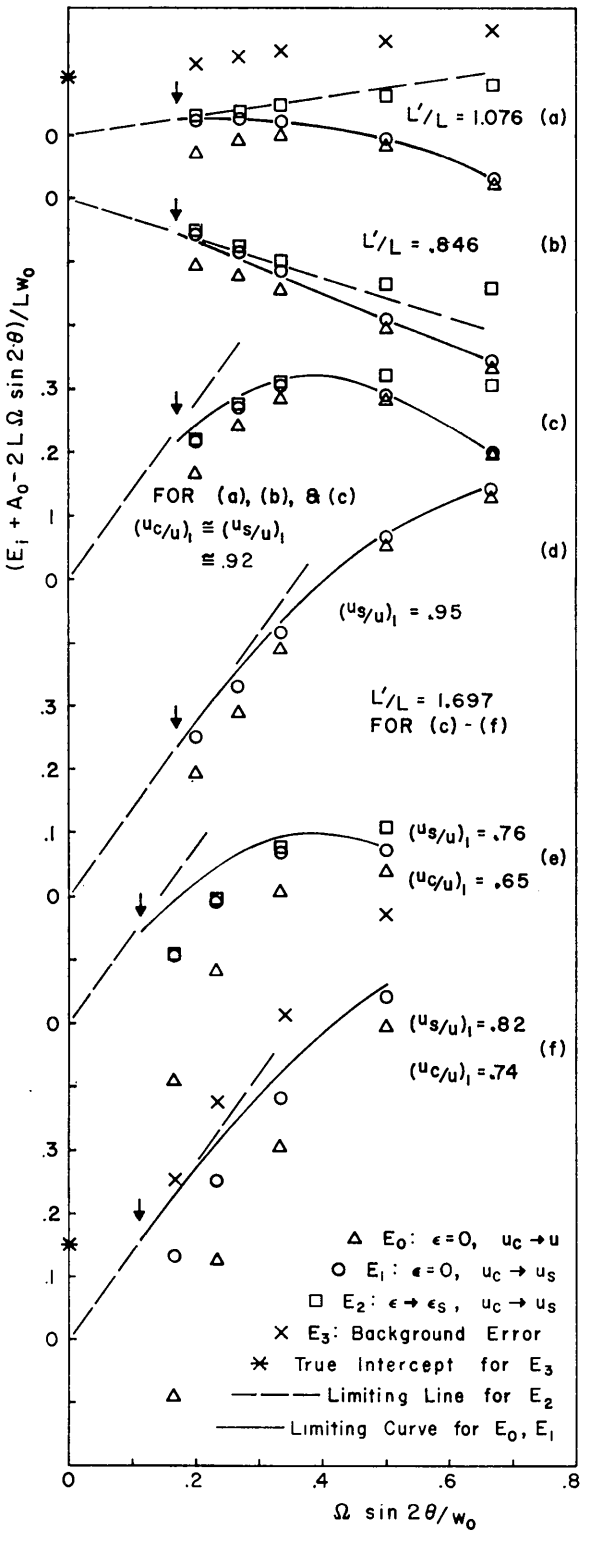

The above illustrations made use of the weighting function W_1, for which the standard deviation is only $\frac{1}{12}$ the minimum scan. Let us now consider the most unfavorable case: W_2, for which the standard deviation is $\frac{1}{2}$ the minimum scan. Unfortunately, this case is realized if a wavelength doublet is used. The plots for the isotropic case (not shown) are almost as favorable as in Fig. 4(*a*). For the most anisotropic case, we show in Fig. 4(*e*) and (*f*) the plots which correspond to 4(*c*) and (*d*). One observes that, even using these two plots together, approximation E_0 is virtually worthless, while E_1 or E_2 could give values within 10 – 20% of the correct ones.

We made a few calculations using W_3. As expected, they gave curves which were displaced only a small amount from those of Fig. 4. These small displacements were so nearly independent of scan length that the effect could not be displayed on the scale of Fig. 4.

A guide to the size of the errors (arising from the weighting function) is given by the amount by which u_C differs from u. In Fig. 4 we give values of u_C/u for the smallest scans. In an actual experiment only the approximation u_S would be known; it is the difference between u_C and u_S which gives rise to errors in the method. We also give values of u_S/u in Fig. 4. We see, for the examples considered, that when u_S/u is greater than, say, 0·9, there is only a small error entailed by replacing u_C by u_S. Depending on the amount of anisotropy in the sample, this replacement becomes increasingly less satisfactory as u_S/u deviates further from unity.

Fig. 4. Plots to determine the unknown TDS fraction using the small scan approximation. The points can be determined from experimental data alone, using various approximations discussed in the text. Except for the case E_3, the points would fall on the curves if it were possible to choose u_C correctly. For a usual length of scan, the TDS fraction is approximately unity in the units used and the degree to which the points can be extrapolated to the same intercept as the curves is a measure of the accuracy of the method. For E_3, the points should extrapolate to the marked intercept. The initial slope, $2(L'/L-1)\sin 2\theta$, is a measure of the deviation from the spherical approximation. u_C/u is a measure of the effect of the broadening W and u_S/u is the spherical approximation to u_C/u. Values of these ratios for the smallest scans are given. Other values may be estimated by comparing E_0 and E_1 to the curves. The vertical arrows show the smallest scan permitted by the broadening function. w_0 is the width of a standard slit, 3°. The curves are for a wavelength, near 0·7 Å, which yields a Bragg angle of 45°. The various curves are for the following material, reflection (Miller indices and direction normal to diffraction plane), weighting function, slit dimensions, and scan type: (*a*) tungsten, (600) – [001], W_1, 3° × 3°, normal ($\psi = 90°$). (*b*) β-brass, (440) – [001], W_1, 3° × 3°, normal. (*c*) β-brass, (440) – [110], W_1, 3° × 3°, θ:2θ. (*d*) same, except 6° × 6° slit. (*e*) same, except W_2 and 3° × 3° slit. (*f*) same, except 6° × 6° slit. For the wide slit cases (*d*) and (*f*), E_2 is negligibly different from E_1.

Experimental considerations

For the reason mentioned, our illustrations have been based on simulated experimental data. We now discuss some of the considerations necessary in an actual experiment. The extent to which each of these need be taken into account depends on individual requirements.

Units: Almost all of our discussion has made use of units such that areas, such as those in Fig. 3(*c*), are expressed as fractions of the integrated Bragg reflection reduced by the factor Lw. Furthermore, in Fig. (4), the experimental quantity E has been altered by a term A_0 $2L \sin 2\theta$. These reduction parameters have been included here for pedagogic reasons only. In actual practice, the natural units would be used; so far as the determination of the included TDS area, one could use count-degrees per second.

Angular factors: We have assumed throughout that the angular factor $F^2 \sin^2 \theta$ varies inappreciably from its value at the relp. If the variation of this quantity is significant, the natural correction is to divide each datum by $F^2\sin^2\theta/F_B^2\sin^2\theta_B$, where the subscript refers to values at the Bragg condition.

Scan type: The interpretation of the TDS will in general be simpler if the surfaces of the active volume are as far as possible from positions where the weighting function is large. Since this condition is equivalent to keeping the Bragg reflection centered in the slit, it is not in general incompatible with other considerations. Scans lying in the range between A and B in Fig. 2 are perfectly satisfactory; both are illustrated in Fig. 4. Scans lying outside this range would be less easy to interpret.

Separation of Bragg and TDS power: The analysis assumes the separability of the Bragg from the TDS power: the former is required to give the weighting function W and it is essential that the shape of the latter not be influenced by the wings of the Bragg peak. Obtaining W to sufficient accuracy would not usually be a problem, especially since much of the information could be obtained at low angle where the TDS is small. The power in the wings of the Bragg reflection can be determined from an investigation of the distribution of power in reciprocal space: for example, the true wings lie along rekhas perpendicular to the faces of the sample; wavelength spreading along a radius; mosaic spreading normal to a radius. Such an investigation would then allow a separation of the Bragg wings from the TDS.

Background level: The application of the method also requires that the first order TDS from acoustic modes be separated from the 'background', which consists of Compton scattering, air scattering, fluorescence, dark current, TDS from optic modes, *etc.* These latter all vary slowly with angle, or can, at least, be corrected to a slow variation with angle. Their value is determined from the power at the ends of a long scan, *e.g.* of twice the width of the slit.

Because both the desired area and assumed power (A_0 and P in Fig. 3) are similarly affected by an error in the choice of background level, this choice is not very critical. In fact, it is easily seen that, to the extent that $u_C/u=1$, the entire analysis is independent of the background level. To illustrate this result, we have considered how the points in Fig. 4(*a*) and (*f*) would be influenced by an error in the choice of background level of three times the TDS power at the ends of the long scan suggested above. (This illustration is of an unrealistically large error. Use of a realistic error would give effects too small to see on Fig. 4.) The points of E_2, altered to show the effect of such a background error, are plotted as E_3. To be sure, the points are displaced a significant amount. The required intercept is displaced a similar amount, however, as shown in the Figure. One can see that the additional error because of an incorrect choice of background would be negligible.

Multiphonon scattering: The higher order phonon processes also produce a diffuse scattering which peaks at a relp. The magnitude is smaller than that from first order scattering. The second order scattering could, in principle, be estimated using preliminary values of L' and the methods described by Warren (1969), but if such high accuracy were required it would probably be better to make a separate study of the elastic properties of the crystal.

6. Summary

Because of the peaking of TDS, measurements of integrated Bragg reflections contain an unwanted component. Suitable notation is shown in Fig. 3 where areas are measured as fractions of the Bragg reflection. The magnitude of the unwanted component is determined by geometrical parameters defined in Fig. 1 and by sample parameters $K_H(\chi)$ referred to in equation (1). Simplification may be achieved by replacing K_H by the completely averaged parameter L [equation (2)] or the partially averaged parameter L' [equation (7)]

The appropriate method for evaluating the unwanted component depends on the accuracy required, the availability of elastic constant data, the tolerability of subsidiary experimental work, and the availability of computer time. We therefore outline the various possibilities.

Elastic constants known

The general formulation is given by Rouse & Cooper (1969). The computer program of Walker & Chipman (1970) takes into account the most important terms, first order TDS and experimental resolution, and is of manageable proportions. If the sample is approx-

imately isotropic or if an accuracy of 15 –50% is all that is required, it is simpler to calculate K_{avg} and proceed with the spherical approximation, below. If an accuracy of 5 – 20% is required, calculate K'_{avg} for each reflection and use the small scan approximation, below.

Average sound velocity known

Spherical approximation: If K_{avg} cannot be evaluated exactly, it may be estimated from equation (9), from the Debye temperature (obtained, for example, from preliminary temperature factors), or otherwise. The unknown areas in Fig. 3 may then be read directly from Fig. 2. A convolution with the experimental resolution function would be possible, but would not usually be warranted.

Small scan approximation: If K'_{avg} cannot be evaluated exactly, it may be estimated from equation (8), from the Debye temperature, or otherwise. For small scans, with negligible experimental broadening, the unknown area may be evaluated immediately from equation (7). In contrast to the spherical approximation, this procedure is 'exact' if K'_{avg} is known, and it may well be worth while to consider experimental broadening. Most of § 5 is devoted to this problem as summarized below.

No elastic constant information: In this case, one might obtain information by measuring the Debye–Waller factor and proceeding as above. Alternatively, and more accurately, it is possible to determine the unknown coefficient in the small scan approximation from the experimental data itself. The basic idea is that the form of the TDS power at moderate scans determines the form concealed by the Bragg peak. In the case that there is negligible experimental broadening the method is easy to apply. When there is broadening it is necessary to make approximations. We have formulated the problem in such a fashion that the convolution of the resolution function with the unknown sample parameter is replaced by a convolution with spherically averaged parameters. The accuracy is illustrated in Fig. 4.

I thank D. R. Chipman & especially C. B. Walker for numerous clarifying discussions, for suggestions concerning the presentation of the results, and the use of their computer program.

APPENDIX

Spherical approximation

Although the necessary formulae have been presented by Skelton & Katz (1969), our notation and point of view is somewhat different. Therefore, we state the required integrals in terms of the parameters defined in Fig. 1 and equation (5). Each integral gives, for a symmetrical scan, the sum of contributions from opposite faces of the active volume; the total included contribution is the sum of $I1$ and $I2$.

$$R=\Omega \sin 2\theta/w \tag{A1a}$$

$$Q=h/w \tag{A1b}$$

$$N=\sin \psi \tag{A1c}$$

$$M=R/N \tag{A1d}$$

$$\frac{\alpha_S}{Lw}=\frac{2RQ}{\pi}\int_0^1 \frac{dx}{\sqrt{(Qx)^2+R^2}}\,\mathrm{Tan}^{-1}\frac{2\sqrt{(Qx)^2+R^2}}{(Qx)^2+M^2-1} \tag{A2}$$

$$\frac{\alpha_{I1}}{Lw}=\frac{2QN}{\pi}\int_0^1 \frac{dx}{\sqrt{(Qx)^2+T^2}}\,\mathrm{Tan}^{-1}\frac{2M\sqrt{(Qx)^2+N^2}}{(Qx)^2-M^2+1} \tag{A3}$$

$$\frac{\alpha_{I2}}{Lw}=\frac{2Q}{\pi}\int_0^1 \frac{dx}{\sqrt{x^2+(Q/N)^2}}\,\mathrm{Tan}^{-1}\frac{2R\sqrt{x^2+(Q/N)^2}}{x^2+Q^2-M^2} \tag{A4}$$

For small scans, equation (A2) is not convenient. One may write instead

$$\frac{\alpha_S}{Lw}=R\left[\ln\frac{G+1+\sqrt{M^2+2G+1}}{G-1+\sqrt{M^2-2G+1}}-\frac{2}{\pi}\int_0^Y \frac{x\,dx}{\sin x}\right]+O\left(\frac{R^2w^2}{h^2}\right) \tag{A5}$$

with

$$G=M\cos\psi \tag{A6a}$$

$$Y=2\tan^{-1}(w/h) \tag{A6b}$$

The integral in (A5) depends only on the slit shape and may be evaluated from Table 1.

Table 1. *Evaluation of* $I=\int_0^Y (x/\sin x)dx$ *with* $Y=2\tan^{-1}(w/h)$.

Set $I=(2w/h)(1-\gamma w^2/h^2)$. Then I may be evaluated for various $w/h=1/Q$, using these γ values.

w/h	γ
0	0·1111
0·2	0·1095
0·4	0·1052
0·6	0·0989
0·8	0·0916
1·0	0·0840
1·2	0·0767
1·4	0·0699

Small scan approximation

Comparison of equations (11) to (14) shows that the correction parameters ε, u_{CH}, and u_{CL} are given by

$$\varepsilon=\int W(x)\left\{\frac{\alpha_I(2u_H-2x)+\alpha_I(2u_L+2x)}{4L'\Omega\sin 2\theta}-1\right\}dx \tag{A7}$$

$$u_{CH}=\frac{\int W(x)\alpha_S(2u_H-2x)\mathrm{d}x}{\int W(x)\dfrac{\alpha_S(2u_H-2x)}{u_H-x}\mathrm{d}x} \tag{A8}$$

$$u_{CL}=\frac{\int W(x)\alpha_S(2u_L+2x)\mathrm{d}x}{\int W(x)\dfrac{\alpha_S(2u_L+2x)}{u_L+x}\mathrm{d}x} \tag{A9}$$

The explicit arguments of the α's are Ω values; the other parameters are understood.

Since the α's may not be known, our approximation is to replace them with the spherically averaged values. The term in braces in (A7) may then be obtained as the difference between the appropriate curve and its asymptote in Fig. 2(*b*), or analytically from (A3) and (A4). The terms in (A8) and (A9) may be read from Fig. 2(*a*) or evaluated from (A5), (A2), or (6). Surprisingly, the needed quantities may be obtained with sufficient accuracy from the Figure, but the process is somewhat tedious.

References

COCHRAN, W. (1969). *Acta Cryst.* A**25**, 95.

COOPER, M. J. & ROUSE, K. D. (1968). *Acta Cryst.* A**24**, 405.

JAMES, R. W. (1948). *The Optical Principles of the Diffraction of X-Rays*. London: Bell.

JENNINGS, L. D. (1969). *J. Appl. Phys.* **40**, 5038.

RAMACHANDRAN, G. N. & WOOSTER, W. A. (1951). *Acta Cryst.* **4**, 335.

ROUSE, K. D. & COOPER, M. J. (1969). *Acta Cryst.* A**25**, 615.

SKELTON, E. F. & KATZ, J. L. (1969). *Acta Cryst.* A**25**, 319.

WALKER, C. B. & CHIPMAN, D. R. (1969). *Acta Cryst.* A**25**, 395.

WALKER, C. B. & CHIPMAN, D. R. (1970). *Acta Cryst.* In the press.

WARREN, B. E. (1969). *X-Ray Diffraction*, p. 165. Reading, Massachusetts: Addison-Wesley.

Acta Cryst. (1970). A**26**, 622

Algorithm for Determining the Symmetry and Stacking Properties of the Planes (*hkl*) in a Bravais Lattice

BY B. GRUBER

Faculty of Mathematics and Physics, Charles University, Prague, Czechoslovakia

(*Received* 1 *July* 1969 *and in revised form* 29 *January* 1970)

An algorithm is presented which enables one to determine in detail the symmetry and stacking properties of the planes (*hkl*) in an arbitrary Bravais lattice characterized by the quantities a, b, c, $\cos\alpha$, $\cos\beta$, $\cos\gamma$.

1. Introduction

The problem of mapping a lattice plane was originally formulated and solved by Jaswon & Dove (1955) and more recently, using the tensor formalism, by Bevis (1969). Nevertheless we believe that it is worth considering the present procedure since it possesses some new and useful features.

Firstly, all considerations refer to the *symmetry* of the plane (*hkl*) which was discussed neither by Jaswon & Dove nor by Bevis.

Secondly, our results, unlike those of the above authors, are presented in a unique way. This is, of course, important when comparing various calculations and compiling tables. The following example shows it clearly. Jaswon & Dove determine in their paper the configuration of the lattice points in the plane (295) in a primitive cubic lattice to be a parallelogram of edges $\sqrt{29}$ and $\sqrt{106}$ and included angle $\cos^{-1}18/(\sqrt{29}\times 106)$. This parallelogram contains four interior lattice points in addition to those at its corners. If they applied their procedure to the equivalent planes (952) and (259) they would have obtained quite different parallelograms with 1 and 8 interior lattice points, respectively. Alternatively the tables obtained from our algorithm give the cell of edges $\sqrt{19}$ and $\sqrt{6}$ and included the angle $\cos^{-1}(\sqrt{114}/57)$. These numbers are unique, since the cell is primitive and has the shortest possible perimeter. Also the symmetry of the plane can be readily recognized. Moreover it is not immediately patent that the results by Jaswon & Dove and ourselves are identical.

Similar comment applies to the procedureof Bevis. Though the resulting parallelogram here is without interior points, its shape depends on the choice of the integers m_1, m_2, m_3 satisfying the Diophantine equation

$$m_1u^1+m_2u^2+m_3u^3=1\ .$$

But this equation has infinitely many solutions provided the u^i are integers without common factor.

Thirdly our procedure is formulated as an algorithm and this way has some advantages, too. The greatest, of course, is the possibility of applying a computer